Multilevel and Multicomponent Layer-by-Layer Assembly for the Fabrication of Nanofibrillar Films

Yuanyuan Zhang and Junqi Sun*

State Key Laboratory of Supramolecular Structure and Materials, International Joint Research Laboratory of Nano-Micro Architecture Chemistry (NMAC), College of Chemistry, Jilin University, Changchun 130012, People's Republic of China

ABSTRACT In this study, we demonstrate multilevel and multicomponent layer-by-layer (LbL) assembly as a convenient and generally applicable method for the fabrication of nanofibrillar films by exploiting the dynamic nature of polymeric complexes. The alternate deposition of poly(allylamine hydrochloride)—methyl red (PAH-MR) complexes with poly(acrylic acid) (PAA) produces nanofibrillar PAH-MR/PAA films, which involves the disassembly of PAH-MR complexes, the subsequent assembly of PAH with PAA, and the PAA-induced assembly of MR molecules into MR nanofibrils via a $\pi-\pi$ stacking interaction. The aqueous solution of weak polyelectrolyte PAA with a low solution pH plays an important role in fabricating nanofibrillar PAH-MR/PAA films because proton transfer from acidic PAA to MR molecules induces the formation of MR nanofibrils. The generality of the multilevel and multicomponent LbL assembly is verified by alternate assembly of complexes of 1-pyrenylbutyric acid (PYA) and PAH with PAA to fabricate PAH-PYA/PAA films with organized nanofibrillar structures. Unlike the traditional static LbL assembly, the multilevel and multicomponent LbL assembly is dynamic and more flexible and powerful in controlling the interfacial assembly process and in fabricating composite films with sophisticated structures. These characteristics of multilevel and multicomponent LbL assembly will enrich the functionalities of the LbL-assembled films.

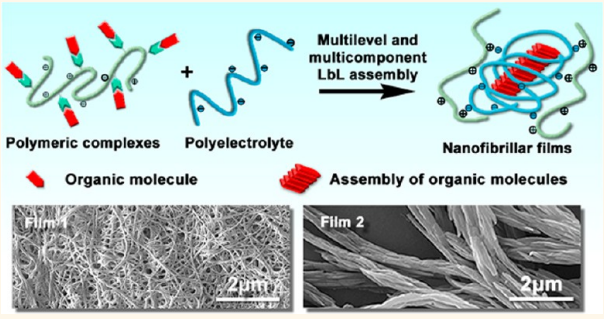

KEYWORDS: layer-by-layer assembly · multilevel assembly · nanofibrillar film · polyelectrolytes · polymeric complexes

Self-assembly of molecules through noncovalent interactions provides a sophisticated way to construct supramolecular materials with unique properties and functions, such as stimuli-responsiveness,[1−4] self-healing,[2,5] adaptation,[6−8] recognition,[9,10] transport,[11,12] and catalysis.[13,14] In the past two decades, new concepts have been continuously introduced to promote the progress of molecular self-assembly, thereby leading to supramolecular assemblies with high levels of precision and complexity and also unprecedented properties.[1,6,15−18] Currently, multilevel assembly, which comprises several sequential subassemblies within the main assembly, has been the subject of extensive research because it enables the progressive buildup of more complex supramolecular assemblies in a precisely defined way.[6,18−20] In practice, the implementation of a multilevel assembly requires progressive control over the molecular interactions in both spatial (structural) and temporal (dynamic) levels, which are governed by the diversity and the dynamic nature of the noncovalent interactions and the information encoded in molecular building blocks.[6,18−20] The hierarchical self-assembly is an example of a multilevel assembly that uses the subunits produced in each assembly to generate larger and more complex assemblies in the next one.[15,19−22] In nature, hierarchical self-assembly of small components creates numerous complex structures, such as the tobacco mosaic virus,[23] natural collagen,[24] and cellulose.[25] Taking inspiration from examples in nature, multilevel assembly has been purposely employed by material scientists to design complex artificial materials with advanced properties and functions by using synthetic species. Such synthetic species include, but are not limited to, block copolymers,[26,27] hyperbranched polymers,[20] small organic molecules,[28] organic—inorganic hybrids,[29] and colloidal particles.[4,30]

* Address correspondence to sun_junqi@jlu.edu.cn.

Received for review March 26, 2015 and accepted July 8, 2015.

Published online July 08, 2015
10.1021/acsnano.5b01832

The layer-by-layer (LbL) assembly, which involves sequential deposition of components with complementary interactions into multilayers, is a convenient and versatile method for fabricating composite films with precisely controlled structures.[31−34] After two decades of worldwide research, numerous advanced films have been produced by LbL assembly, which include antireflection coatings,[35] superhydrophobic surfaces,[36,37] actuators,[38] self-healing films,[37,39] drug delivery systems,[40,41] separation membranes,[42,43] and so forth.[44−48] The rapid progress of LbL assembly mainly benefited from enriching interactions that drive the multilayer formation,[32,49,50] broadening types of materials that can be manipulated by LbL assembly,[51,52] and developing a rapid LbL assembly technique that enables the convenient fabrication of thick films.[37,53−56] However, the LbL assembly technology requires further development to continuously support the production of films with more complex structures and unprecedented functions. Inspection of the current LbL assembly reveals a gap between the latest developments in self-assembly and the LbL assembly. The integration of new concepts in self-assembly into the method of LbL assembly will provide a practical way to further promote the progress of the LbL assembly technique.[57] Up to now, the majority of LbL-assembled films are fabricated by using dipping solutions with one component in each solution. In our previous work, we have demonstrated that nonstoichiometric polymeric complexes can be LbL-assembled with complementary partner species to produce composite films with self-healing ability,[37,58] enhanced mechanical robustness,[59] high loading capacity,[60] and conveniently tailored micro- and nanostructures.[37,51,58] These functional films benefit from the increased composition and structural diversity of polymeric complexes compared with uncomplexed polymers.[53] However, the dynamic nature of polymeric complexes, despite their multiple components, has not been used in the manipulation of multilevel assembly for the fabrication of films with more complicated structures because these previously used polymeric complexes are relatively stable and act as a whole in LbL assembly.[37,51,58−60] The inability of these stable polymeric complexes to dynamically disassemble to participate in assembly with subsequently deposited components prevents the occurrence of multilevel LbL assembly. Therefore, to undergo multilevel LbL assembly, polymeric complexes should show dynamic property, which requires these polymeric complexes to be supported by multiple interactions involving differential forces. The multilevel LbL assembly of polymeric complexes will provide a platform to further tailor structures and enrich functionalities of the LbL-assembled films.

In this study, as a proof-of-concept for multilevel and multicomponent LbL assembly, we demonstrate that the alternate deposition of poly(allylamine hydrochloride)−methyl red (PAH-MR) complexes with poly(acrylic acid) (PAA) produces nanofibrillar films. When the deposited PAH-MR complexes are immersed in aqueous PAA solution, the disassembly of PAH-MR complexes and the reassembly of PAH with PAA lead to the liberation of MR molecules. The liberated MR molecules further self-assemble into nanofibrils within the PAH/PAA film, in which PAA provides an acidic microenvironment. The multilevel and multicomponent LbL assembly is further extended to fabricate composite films comprising 1-pyrenylbutyric acid (PYA) nanofibrils by LbL assembly of PAH-PYA complexes with PAA, demonstrating its generality for fabricating films with enriched structures.

RESULTS AND DISCUSSION

Fabrication of PAA/PAH-$MR_{0.2}$ Nanofibrillar Films. The chemical structures of PAH and MR are shown in the inset of Figure 1. PAH complexes with MR through the electrostatic and hydrogen-bonding interactions between amine groups of PAH and carboxylic acid groups of MR. With a feed monomer molar ratio of PAH to MR of 1:0.2, the aqueous solution of PAH-$MR_{0.2}$ complexes with a pH of 7.5 is stable at room temperature for at least 2 months. As shown in Figure 1, the dynamic light scattering (DLS) curve of a PAH-$MR_{0.2}$ aqueous solution exhibits a polydisperse but monomodal distribution with a *z*-average hydrodynamic diameter of ~92 nm. The PAH-$MR_{0.2}$ complexes have a ζ-potential of +50.7 mV, indicating that the outer surface of the complexes has a high amount of PAH. The positively charged PAH-$MR_{0.2}$ complexes (pH 7.5) can be LbL assembled with PAA (pH 3.5) to produce (PAA/PAH-$MR_{0.2}$)*n films. The (PAA/PAH-$MR_{0.2}$)*30 film appears red, indicating the successful incorporation of MR molecules into the film (Figure 2a). The scanning electron microscopy (SEM) images in Figure 2b and c indicate that the surface of the (PAA/PAH-$MR_{0.2}$)*30 film is covered with randomly aligned nanofibrils with an average diameter of 58.3 ± 17.3 nm. The enlarged SEM image in Figure 2c clearly shows that polymeric films are present in the interstices of nanofibrils, which glue or

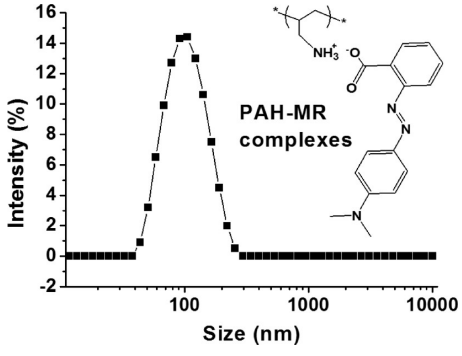

Figure 1. Hydrodynamic diameter distribution curve of PAH-$MR_{0.2}$ complexes in aqueous solution with a pH of 7.5. The inset presents the chemical structures of PAH and MR.

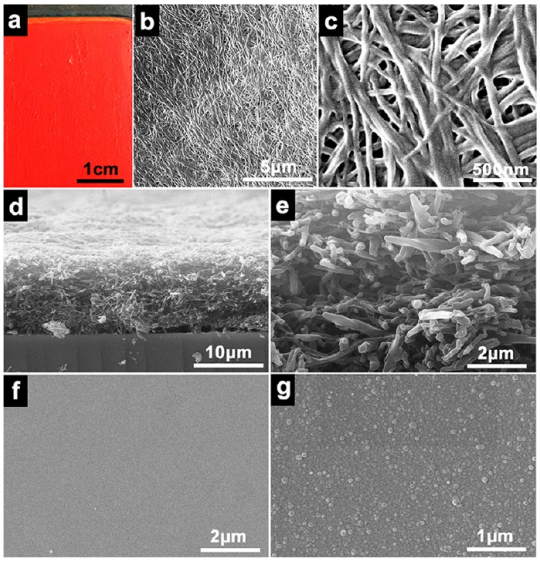

Figure 2. (a) Photograph of a (PAA/PAH-$MR_{0.2}$)*30 film. (b, c) Top-view SEM images of a (PAA/PAH-$MR_{0.2}$)*30 film. (d, e) Cross-sectional SEM images of a (PAA/PAH-$MR_{0.2}$)*30 film. (f, g) Top-view SEM images of a (PAA-7.5/PAH-$MR_{0.2}$)*30 film (f) and a (PSS-3.5/PAH-$MR_{0.2}$)*30 film (g).

wrap neighboring nanofibrils together. The cross-sectional SEM in Figure 2d and e further reveal that not only the film surface but the entire film is composed of nanofibrils. These nanofibrils lie horizontally on the substrate surface and randomly stack into a continuous nanofibrillar film.

To understand the factors that govern the formation of nanofibrillar films, the pH of the PAA dipping solution was changed from 3.5 to 7.5 to fabricate the (PAA-7.5/PAH-$MR_{0.2}$)*n film (7.5 after PAA indicates the pH of the PAA dipping solution). As shown in Figure 2f, a smooth (PAA-7.5/PAH-$MR_{0.2}$)*20 film with a thickness of 70.8 $\pm$ 9.6 nm was obtained, indicating that the fabrication of nanofibrillar PAA/PAH-$MR_{0.2}$ films is dependent on the pH of the PAA dipping solution. Meanwhile, the characteristic absorbance of MR molecules at 428 nm is relatively low in the (PAA-7.5/PAH-$MR_{0.2}$)*20 film (Supporting Information, Figure S1a). When the deposited PAH-$MR_{0.2}$ complexes were transferred into an aqueous PAA solution with higher pH, MR molecules were protonated and their electrostatic interaction with PAH was weakened. Therefore, the release of the already deposited MR molecules becomes prominent, thereby leading to a low loading amount of MR into the (PAA-7.5/PAH-$MR_{0.2}$)*20 film. In another controlled experiment, an aqueous PAA solution with a pH of 3.5 is replaced with an aqueous PSS solution (1 mg/mL) with the same pH value. The (PSS-3.5/PAH-$MR_{0.2}$)*n films are fabricated following the same procedure used for the fabrication of (PAA/PAH-$MR_{0.2}$)*n films. Instead of nanofibrils, nanoparticles with an average size of 430 nm are observed on the surface of the (PSS-3.5/PAH-$MR_{0.2}$)*20 film (Figure 2g). The UV−vis absorption spectrum of the (PSS-3.5/PAH-$MR_{0.2}$)*20 film confirms the incorporation of MR molecules in the films (Supporting Information, Figure S1b). The nanoparticles are aggregates of PAH-$MR_{0.2}$ complexes glued with PSS. These controlled experiments confirm that weak polyelectrolyte PAA with a low solution pH serves an important function in the fabrication of nanofibrillar films.

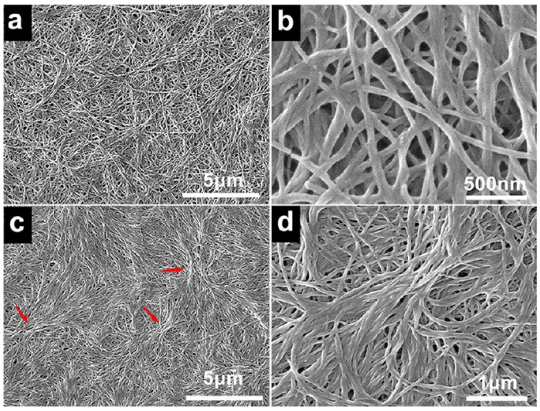

Figure 3. SEM images of MR nanofibrils produced in aqueous MR solution (a, b) and PAH-$MR_{0.2}$ complex solution (c, d). The arrows in (c) indicate the radial centers of the nanofibrils.

MR Nanofibrils in Aqueous Solutions and Solid Films. Previously reported PAA/PAH films fabricated by LbL assembly do not contain any nanofibrils.[35,38] Thus, the formation of nanofibrils in (PAA/PAH-$MR_{0.2}$)*30 is believed to be highly related to the MR molecules. An aqueous HCl solution is added into the aqueous MR solution (2 mM) with a starting pH of 7.5, and flocculent red MR precipitates appear immediately when the solution pH drops to lower than pH 7.0. SEM images in Figure 3a and b show that the precipitates are MR nanofibrils with an average diameter of 60.1 $\pm$ 10.4 nm. Moreover, red MR nanofibrils also precipitate from aqueous PAH-$MR_{0.2}$ solution (2 mM, pH 7.5) with the addition of an aqueous HCl solution. The MR nanofibrils have an average diameter of 58.4 $\pm$ 8.4 nm (Figure 3c and d), and those produced in aqueous MR solution have nearly the same average diameter. Therefore, the complexation of MR with PAH cannot prevent the formation of MR nanofibrils. Close examination of SEM images in Figure 3 reveals that the MR nanofibrils prepared in MR solution are randomly arranged, and the nanofibrils prepared in PAH-$MR_{0.2}$ solution have a radial structure with clearly recognizable radial centers.

X-ray diffraction (XRD) measurements were performed on MR nanofibrils prepared from aqueous MR and PAH-$MR_{0.2}$ solutions to characterize their structures. The diffraction peaks indicate that the MR nanofibrils are composed of MR nanocrystals (Figure 4a, I and II). The diffraction peak at 25.2° (Figure 4a), which corresponds to a d spacing of 3.5 Å, matches well with the $\pi-\pi$ stacking distance of typical π-conjugated molecules.[61] This result suggests that the MR nanofibrils

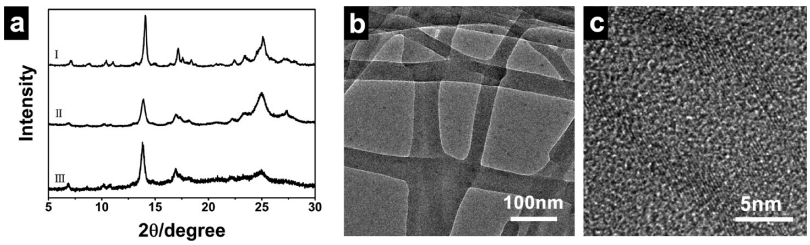

Figure 4. (a) XRD patterns of MR nanofibrils prepared from aqueous MR solution (I), PAH-$MR_{0.2}$ complex solution (II), and (PAA/PAH-$MR_{0.2}$)*30 film (III). (b, c) TEM (b) and HRTEM (c) images of MR nanofibrils prepared from an aqueous MR solution.

are constructed via a $\pi-\pi$ stacking interaction. The XRD patterns of the (PAA/PAH-$MR_{0.2}$)*30 film show the same crystal structure in the nanofibrils prepared in aqueous MR and PAH-$MR_{0.2}$ solutions (Figure 4a III). However, the diffraction peak at 25.2° in the (PAA/PAH-$MR_{0.2}$)*30 film is broader and weaker than that in nanofibrils prepared in MR and PAH-$MR_{0.2}$ solutions, thereby indicating that the crystallinity of MR nanofibrils decreases with the introduction of PAA and PAH polyelectrolytes. Differential scanning calorimetry (DSC) measurements show that the melting temperatures of MR nanocrystals decrease in the sequence of nanofibrils prepared in MR solution, in PAH-$MR_{0.2}$ solution, and in (PAA/PAH-$MR_{0.2}$)*30 film, further confirming that the introduction of polyelectrolytes decreases the crystallinity of the MR nanofibrils (Supporting Information, Figure S2). The MR nanofibrils prepared from MR solution have the highest crystallinity and are selected for further examination by transmission electron microscopy (TEM). Figure 4b shows the low-magnification TEM image of the MR nanofibrils, whose morphology is consistent with that observed by SEM. The (HR)TEM image in Figure 4c further indicates that the MR nanofibrils are composed of tiny MR nanocrystals and amorphous MR. Therefore, the formation of the MR nanofibrils in solutions and solid films involves a crystalline process. In an aqueous solution of PAH-$MR_{0.2}$ complexes, MR crystalline nuclei are produced within the complexes when the solution pH is decreased. The MR nuclei are confined to the PAH-$MR_{0.2}$ complexes; thus, nanofibrils growing from these nuclei have a radial structure. By contrast, the homogeneously distributed MR crystalline nuclei in aqueous MR solution result in randomly oriented nanofibrils. This explains the morphological difference of MR nanofibrils prepared in aqueous MR and PAH-$MR_{0.2}$ complex solutions.[62]

Process for the Formation of Nanofibrillar PAA/PAH-$MR_{0.2}$ Films. The morphologies of the (PAA/PAH-$MR_{0.2}$)*n films with different deposition cycles were investigated with SEM to clarify the formation of the nanofibrillar films. Before the fourth deposition cycle, continuous PAA/PAH-$MR_{0.2}$ films with granular aggregates instead of nanofibrils are observed. The typical aggregates in the (PAA/PAH-$MR_{0.2}$)*4 films are composed of particles that are 50.9 ± 10.2 nm in size, and these are assumed to be PAH-$MR_{0.2}$ complexes glued with PAA (Figure 5a). The shrinking of PAH-$MR_{0.2}$ complexes in the aggregates compared with those in aqueous solution is caused by the partial loss of hydrated water. Dandelion-like aggregates of MR nanofibrils radiating from the granular aggregates appear starting from the fifth deposition cycle (Figure 5b). In the (PAA/PAH-$MR_{0.2}$)*5.5 film (Figure 5c), the deposition of PAA is recognized by the wormlike aggregates on the continuous film (Figure 5c3), and such aggregates are not observed in the (PAA/PAH-$MR_{0.2}$)*5 film with the PAH-$MR_{0.2}$ complexes as the outermost layer (Figure 5b2). Compared with the (PAA/PAH-$MR_{0.2}$)*5 film, the deposition of the PAA layer does not change the density and size of the nanofibrils, indicating that the growth of nanofibrils takes place in the dipping solution of PAH-$MR_{0.2}$ complexes. After immersion of the (PAA/PAH-$MR_{0.2}$)*4.5 film in an aqueous solution of PAH-$MR_{0.2}$ complexes for 1 min, incomplete dandelion-like aggregates of MR nanofibrils with sizes less than ~8 μm were obtained (Supporting Information, Figure S3). The growth of the MR nanofibrils continues up to 15 min immersion in PAH-$MR_{0.2}$ solution, and thereafter no nanofibril growth was observed even when immersion was extended to 2 h. With an increasing number of film deposition cycles, the MR nanofibrils grow longer and new MR nanofibrillar aggregates are also produced (Figure 5d, e, and f). The neighboring MR nanofibrillar aggregates are gradually interwoven fully to produce a continuous nanofibrillar film (Figure 5f). Although the length of the MR nanofibrils depends on the number of film deposition cycles, the diameter of the MR nanofibrils remains unchanged with increasing number of film deposition cycles. UV−vis absorption spectra show that MR molecules leach out into the PAA dipping solution during LbL assembly of the nanofibrillar (PAA/PAH-$MR_{0.2}$)*n films. The MR molecules in the PAA dipping solution can suppress the further dissolution of the MR molecules from PAA/PAH-$MR_{0.2}$ films and accelerate the deposition process of the (PAA/PAH-$MR_{0.2}$)*n films. In a control experiment, a (PAA/PAH-$MR_{0.2}$)*15 film was fabricated by replacing the PAA dipping solution with a fresh one after each film deposition cycle. The thickness of the (PAA/PAH-$MR_{0.2}$)*15 film with the PAA dipping solution being replaced corresponds to that of the (PAA/PAH-$MR_{0.2}$)*12 film without the PAA dipping solution being replaced. However, the diameter of the MR nanofibrils

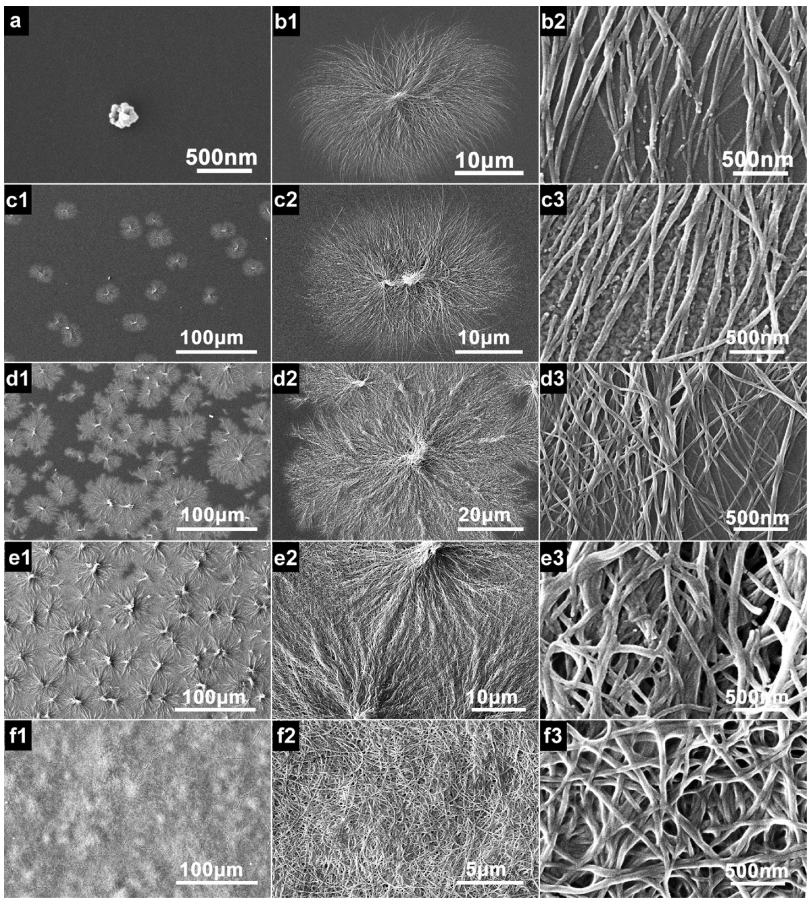

Figure 5. SEM images of (PAA/PAH-MR$_{0.2}$)*n films with n = 4 (a), 5 (b), 5.5 (c), 7 (d), 9 (e), and 15 (f).

shows no difference for the (PAA/PAH-MR$_{0.2}$)*15 films with and without the PAA dipping solutions being replaced.

To confirm the existence of PAA and PAH in the nanofibrillar PAA/PAH-MR$_{0.2}$ films, a (PAA/PAH-MR$_{0.2}$)*30 film was etched in ethanol to selectively dissolve MR nanofibrils. After immersion in ethanol for 1 h, the red color of the film completely disappeared, thereby confirming the removal of MR nanofibrils from the film. Then, the resultant film was heated at 180 °C for 2 h. The Fourier transform infrared (FT-IR) spectrum of the thermally treated film shows the amide I peak at ~1650 cm^{-1}, indicating that thermal treatment leads to the formation of amide bonds between the amine and carboxylic acid groups (Supporting Information, Figure S4).[38] The MR molecules are removed from the film. Thus, the amide originates from the cross-linkage of PAH amine groups and the PAA carboxylic acid groups, verifying the co-deposition of PAA, PAH, and MR in the PAA/PAH-MR$_{0.2}$ films. Moreover, thermogravimetric analysis (TGA) measurements were performed on PAA/PAH-MR$_{0.2}$ and PAA/PAH films scratched from substrates and MR nanofibrils that are directly prepared from aqueous MR solution. The MR nanofibrils show faster decomposition behavior than the PAA/PAH film (Supporting Information, Figure S5). The PAA/PAH-MR$_{0.2}$ film shows the characteristic decomposition behaviors of MR nanofibrils and a PAA/PAH film in temperature ranges of 200 to 250 °C and 400 to 470 °C, respectively. This result also confirms the existence of PAA, PAH, and MR in the PAA/PAH-MR$_{0.2}$ films. Previous studies have demonstrated that microporous films can be created by immersing PAA/PAH films into acidic aqueous solution because of the pH-induced phase separation.[63,64] When (PAA/PAH-MR$_{0.2}$)*20 films were immersed into one of the acidic aqueous solutions (pH 2.4, 2.5, and 2.6) for 60 s and then rinsed with neutral water for about 15 s, no micropores were developed on the (PAA/PAH-MR$_{0.2}$)*20 films. This might be because the PAA/PAH films are thin and confined in the interstices of MR nanofibrils.

Mechanism for the Formation of Nanofibrillar Films. On the basis of the above-mentioned results, we can confirm that the formation of the nanofibrillar PAA/PAH-MR$_{0.2}$ films involves the crystallization of MR nanofibrils, which requires the assistance of acidic PAA. Therefore, the mechanism of the formation of nanofibrillar PAA/PAH-MR$_{0.2}$ films is proposed as follows (Figure 6). In the initial deposition cycles (within 4 deposition cycles), the alternate deposition of PAH-MR$_{0.2}$ complexes and PAA gradually induces the formation of MR crystal nuclei (Figure 6a), which are important for MR nanofibril growth. When the substrate with the MR crystal

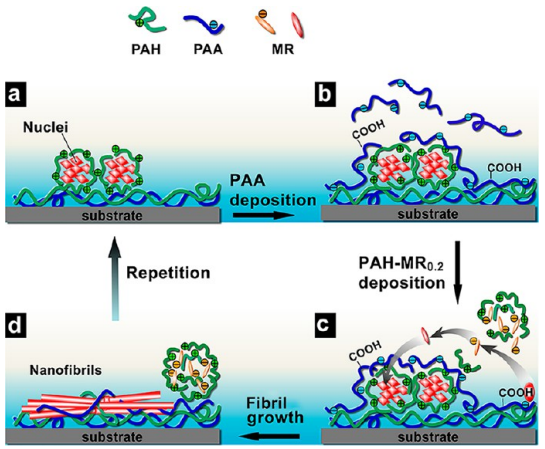

Figure 6. Schematic illustration of the formation of the PAA/PAH-$MR_{0.2}$ nanofibrillar film.

nuclei is immersed in acidic aqueous PAA solution, protonated PAA is deposited onto PAH-$MR_{0.2}$ complexes based on electrostatic and hydrogen bond interactions (Figure 6b). The subsequent deposition of PAH-$MR_{0.2}$ complexes leads to complexation of PAA with PAH, which deprotonates acidic PAA and concomitantly replaces MR molecules in the PAH-$MR_{0.2}$ complexes. The protons in PAA are thereby transferred to MR molecules in the deposited PAH-$MR_{0.2}$ complexes (Figure 6c). The proton transfer during the formation of MR nanofibrils was supported by the following facts. (i) The formation of MR nanofibrils in aqueous solution requires the addition of an aqueous HCl solution. (ii) The LbL assembly of PAH-$MR_{0.2}$ complexes with either neutral PAA or acidic PSS fails to produce MR nanofibrils because neither neutral PAA nor acidic PSS can transfer protons to MR molecules in the films. Upon acceptance of protons, carboxylate groups of MR molecules are protonated and the electrostatic repulsion between them is significantly reduced. Therefore, $\pi-\pi$ interaction among MR molecules is enhanced, thereby driving the formation of MR nanofibrils (Figure 6d). The proton transfer process is verified by FT-IR spectra (Supporting Information, Figure S6). The formation of MR crystal nuclei in the initial deposition cycles follows the same procedure as the formation of MR nanofibrils.

Therefore, a multilevel and multicomponent LbL assembly process is involved in the fabrication of nanofibrillar PAH-$MR_{0.2}$/PAA films. The assembly of PAH and MR in aqueous solution produces PAH-$MR_{0.2}$ complexes. Then, the assembly of PAH-$MR_{0.2}$ complexes with PAA produces PAA-PAH films and simultaneously releases MR molecules. Proton transfer from PAA to the released MR molecules induces the subsequent assembly of MR molecules into nanofibrils. These nanofibrils have electrostatic and hydrogen-bonding interactions with PAA-PAH films and are incorporated into PAA-PAH matrix films. The repeated deposition of PAA and PAH-$MR_{0.2}$ complexes produces thick PAH-$MR_{0.2}$/PAA nanofibrillar films. By replacing PAH with branched

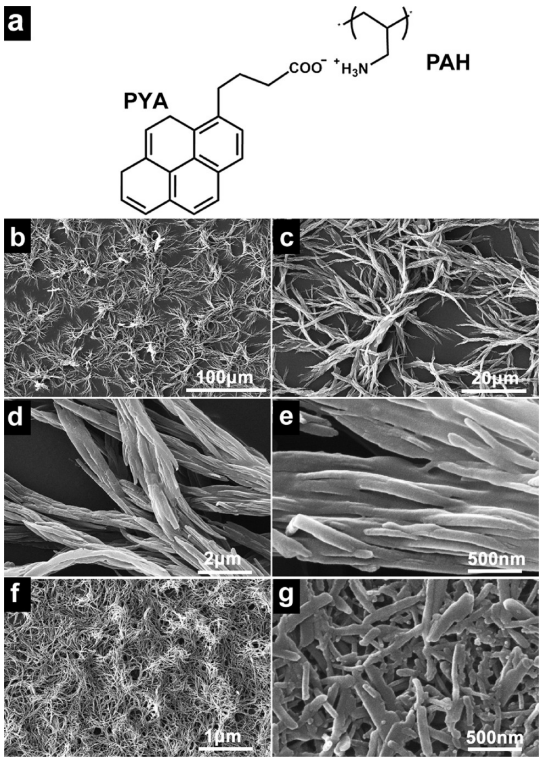

Figure 7. (a) Chemical structures of PAH and PYA. (b–e) Top-down SEM images of a (PAA/PAH-$PYA_{0.3}$)*20 film with different magnification. (f) Top-down SEM image of a (PAA/PAH-$PYA_{0.3}$)*30 film. (g) SEM images of PYA nanofibrils produced in aqueous PYA solution.

polyethylenimine (bPEI), nanofibrillar bPEI-$MR_{0.2}$/PAA films similar to PAH-$MR_{0.2}$/PAA films are fabricated (Supporting Information, Figure S7). The bPEI-PAA matrix in the nanofibrillar bPEI-$MR_{0.2}$/PAA film is more recognizable than the PAH-PAA matrix in the nanofibrillar PAH-$MR_{0.2}$/PAA film. Compared with the previously reported traditional LbL assembly of polymeric complexes, the multilevel-LbL assembly provides more opportunities to fabricate films with more sophisticated structures.

Generality of Multilevel and Multicomponent LbL Assembly. To demonstrate the generality of multilevel and multicomponent LbL assembly in fabricating composite films with sophisticated structures, the LbL assembly of PAA with complexes of PAH and 1-pyrenylbutyric acid (PAH-PYA) is conducted. The PAH-PYA complexes (Figure 7a), which have a monomer molar ratio of PAH to PYA of 1:0.3, were denoted as PAH-$PYA_{0.3}$. DLS measurement shows that PAH-$PYA_{0.3}$ complexes (pH 8.5) have an average hydrodynamic diameter of approximately 154 nm. Similar to PAH-$MR_{0.2}$ complexes, PAH-$PYA_{0.3}$ complexes are positively charged with a ζ-potential of +40.0 mV. The LbL assembly of PAH-$PYA_{0.3}$ complexes with PAA produces white PAH-$PYA_{0.3}$/PAA films. SEM images of a (PAH-$PYA_{0.3}$/PAA)*20 film reveal twisted bunches of fibrils (Figure 7b and c). Enlarged SEM images in Figure 7d and e show that each fibril has a diameter of 0.5 to 1.5 μm, which comprises

nanofibrils that are 96.0 ± 27.3 nm in diameter. These nanofibrils organize themselves in a parallel manner to form fibers of large diameters. The surface of the substrate is fully covered with bunches of fibers when the number of film deposition cycles reaches 30 (Figure 7f).

XRD patterns of a (PAH-$PYA_{0.3}$/PAA)*80 film show a diffraction peak of 23.1° at 2θ (Supporting Information, Figure S8), which corresponds to a *d* spacing of 3.8 Å. This value matches the $\pi-\pi$ stacking distance of pyrene molecules, suggesting that the nanofibrils are built from PYA molecules via $\pi-\pi$ stacking.[61] To clarify the formation of the PYA nanofibrils in PAH-$PYA_{0.3}$/PAA films, the formation of PYA nanofibrils in aqueous PYA solution is also investigated. Short nanofibers with diameters of 95.8 ± 25.0 nm can precipitate from the PYA solution when the pH decreases upon addition of aqueous HCl solution (Figure 7g). Compared with MR nanofibrils precipitated from aqueous MR solution, the PYA nanofibrils are significantly shorter. Similarly, short PYA nanofibrils also precipitate from an aqueous solution of PAH−$PYA_{0.3}$ complexes by decreasing its solution pH. Therefore, we conclude that the formation of nanofibrillar PAH-$PYA_{0.3}$/PAA films follows the same mechanism for the formation of nanofibrillar PAH-$MR_{0.2}$/PAA films. The multilevel and multicomponent LbL assembly of PAH-$PYA_{0.3}$ complexes and PAA involves the disassembly of PAH-$PYA_{0.3}$ complexes, assembly of PAH with PAA, and proton transfer from acidic PAA to PYA, which induces PYA molecule assembly to PYA nanofibrils. These nanofibrils assemble to form large fibrils with the assistance of PAA and PAH polyelectrolytes.

CONCLUSIONS

In summary, we present the first example of multilevel and multicomponent LbL assembly by exploiting the dynamic nature and synergistic effects of the building blocks. The alternate deposition of PAH-$MR_{0.2}$ complexes with acidic PAA produces PAH-$MR_{0.2}$/PAA nanofibrillar films. The formation of a nanofibrillar film involves the disassembly of PAH-$MR_{0.2}$ complexes, the reassembly of PAH with PAA, and the PAA-assisted assembly of MR molecules into MR nanofibrils. The assembly of PAH with PAA liberates the MR molecules from PAH and simultaneously transfers protons in PAA to the MR molecules, thereby inducing the self-assembly of MR molecules into nanofibrils via a $\pi-\pi$ stacking interaction. The dynamic nature of PAH-$MR_{0.2}$ complexes and the differential interactions among these three components serve important functions in enabling the occurrence of a multilevel and multicomponent LbL assembly. The multilevel and multicomponent LbL assembly was further extended to the fabrication of PAH-$PYA_{0.3}$/PAA films with organized fibrillar structures. The multilevel and multicomponent LbL assembly can improve the manner by which LbL assembly is performed to fabricate composite films by manipulating multiple interfacial assemblies of preassembled multicomponent building blocks with a dynamic nature. The application of multilevel and multicomponent LbL assembly is not limited to the examples presented in this study and will provide a new pattern for fabricating composite films with well-controlled sophisticated structures and enriched functionalities.

METHODS

Materials. PAA (M_w ca. 1800), PAH (M_w ca. 56 000), poly(sodium 4-styrenesulfonate) (PSS, M_w ca. 70 000), branched poly(ethylenimine) (bPEI, M_w ca. 25 000), and poly(diallyldimethylammonium chloride) (PDDA, 20 wt %, M_w ca. 100 000−200 000) were purchased from Sigma-Aldrich. MR was purchased from West Long Chemical Reagents Company in China. PYA was purchased from Alfa Aesar. All chemicals were used without further purification. Deionized water was used for all experiments. Solution pH was adjusted with 1 M HCl or 1 M NaOH. The concentrations of PAA and PSS aqueous solutions were set at 1 mg mL^{-1}.

Preparation of PAH-MR and PAH-PYA Complexes. An aqueous MR solution (50 mM) was prepared by dissolving MR (1.347 g, 0.005 mol) in a 60 mM aqueous NaOH solution (100 mL). The aqueous MR solution was injected into aqueous PAH solution (1 mg/mL) with intense stirring to produce the aqueous PAH-MR complex solution with a monomer molar ratio of PAH to MR of 1:0.2 (noted as PAH-$MR_{0.2}$). The final concentration of PAH and MR in aqueous PAH-$MR_{0.2}$ solution was 10 mM and 2 mM, respectively. The pH of the aqueous PAH-$MR_{0.2}$ solution was adjusted to 7.5 by adding HCl. The aqueous PAH-$PYA_{0.3}$ solution with a 1:0.3 monomer molar ratio of PAH to PYA was prepared in a similar way to the PAH-$MR_{0.2}$ solution. The pH of the aqueous PAH-$PYA_{0.3}$ solution was adjusted to 8.5.

Preparation of MR Nanofibrils. MR nanofibrils were precipitated from either aqueous MR or PAH-$MR_{0.2}$ solutions. An aqueous HCl solution (1 M) was gradually added with intense stirring into an aqueous PAH-$MR_{0.2}$ or aqueous MR solution (2 mM). MR flocculent precipitates appeared when the solution pH was slightly below 7.0. The MR precipitates produced in both solutions were then isolated by centrifuging the corresponding dispersions at 3000 rpm. Finally, the centrifuged MR precipitates were carefully washed with deionized water three times and then dried under vacuum in an oven at 30 °C for 24 h. PYA nanofibrils were prepared in a manner similar to the preparation of MR nanofibrils by adding aqueous HCl solution into PYA and PAH-$PYA_{0.3}$ solutions.

Preparation of LbL-Assembled Films. Quartz and silicon substrates were immersed in piranha solution (3:7 mixture of 30% H_2O_2 and 98% H_2SO_4) and heated until no bubbles were released. *Caution: Piranha solution reacts violently with organic materials and should be handled carefully*. The freshly cleaned quartz and silicon wafers were immersed in PDDA aqueous solution (1.0 mg mL^{-1}) for 20 min to obtain a cationic ammonium-terminated surface. The LbL assembly of (PAA/PAH-$MR_{0.2}$)*n films (where n refers to the number of film deposition cycles, and a half cycle means that PAA is the outmost layer) was automatically conducted by a programmable dipping machine (Dipping Robot DR-3, Riegler & Kirstein GmbH) at room temperature. The PDDA-modified substrate was initially immersed in an aqueous PAA solution (pH 3.5) for 15 min to obtain a layer of PAA and then rinsed in four deionized water baths for 1 min each time. The substrate was then immersed in an aqueous PAH-$MR_{0.2}$

solution (pH 7.5) for 15 min and then rinsed in four deionized water baths for 1 min each time. The immersion and rinsing steps were repeated until the desired number of bilayers was obtained. No drying step was conducted in the deposition procedure unless it was in the last layer. By replacing the PAH-$MR_{0.2}$ solution with a PAH-$PYA_{0.3}$ solution, fibrillar PAH-$PYA_{0.3}$/PAA films can be fabricated in the same way as the nanofibrillar PAH-$MR_{0.2}$/PAA films.

Characterization. DLS studies and ζ-potential measurements were carried out on a Malvern Nano-ZS Zetasizer at room temperature. The measurements were made at a scattering angle of $\theta = 173°$ at 25 °C using a He–Ne laser with a wavelength of 633 nm. UV–vis absorption spectra were recorded with a Shimadzu UV-2550 spectrophotometer. SEM images were obtained with a XL30 ESEM FEG scanning electron microscope. All samples were coated with a thin layer of gold (2 to 3 nm) prior to SEM imaging. TEM images were obtained using a Philips Tecnai F20 transmission electron microscope at 200 kV. XRD patterns were measured on a Bruker AXS D8 ADVANCE X-ray diffractometer with Cu Kα radiation (λ = 1.5418 Å). DSC measurements were performed using a Netzsch DSC-204 with a heating rate of 5 °C min^{-1}. TGA curves were obtained on a TGA Pyris Diamond TG/DTA thermogravimeter (PerkinElmer, USA) with a heating rate of 5 °C min^{-1} under an N_2 atmosphere. Digital camera images were captured by a Sony digital video camera recorder (DCR-SR62E).

Conflict of Interest: The authors declare no competing financial interest.

Supporting Information Available: UV–vis absorption spectra of (PAA-7.5/PAH-$MR_{0.2}$)*20 and (PSS-3.5/PAH-$MR_{0.2}$)*20 films; additional DSC, SEM, FT-IR, and TGA characterizations of MR nanofibrils and nanofibrilar films; SEM image of a (PAA/bPEI-$MR_{0.2}$)*30 nanofibrillar film and XRD patterns of a (PAA/PAH-$PYA_{0.3}$)*80 film. The Supporting Information is available free of charge on the ACS Publications website at DOI: 10.1021/acsnano.5b01832.

Acknowledgment. This work was supported by the National Basic Research Program (2013CB834503) and the National Natural Science Foundation of China (NSFC grants 21225419 and 21221063).

REFERENCES AND NOTES

1. Bissell, R. A.; Córdova, E.; Kaifer, A. E.; Stoddart, J. F. A Chemically and Electrochemically Switchable Molecular Shuttle. *Nature* **1994**, *369*, 133–137.
2. Appel, E. A.; Loh, X. J.; Jones, S. T.; Biedermann, F.; Dreiss, C. A.; Scherman, O. A. Ultrahigh-Water-Content Supramolecular Hydrogels Exhibiting Multistimuli Responsiveness. *J. Am. Chem. Soc.* **2012**, *134*, 11767–11773.
3. Nunes, S. P.; Behzad, A. R.; Hooghan, B.; Sougrat, R.; Karunakaran, M.; Pradeep, N.; Vainio, U.; Peinemann, K.-V. Switchable pH-Responsive Polymeric Membranes Prepared *via* Block Copolymer Micelle Assembly. *ACS Nano* **2011**, *5*, 3516–3522.
4. Ma, N.; Li, Y.; Xu, H.; Wang, Z.; Zhang, X. Dual Redox Responsive Assemblies Formed from Diselenide Block Copolymers. *J. Am. Chem. Soc.* **2010**, *132*, 442–443.
5. Cordier, P.; Tournilhac, F.; Soulié-Ziakovic, C.; Leibler, L. Self-Healing and Thermoreversible Rubber from Supramolecular Assembly. *Nature* **2008**, *451*, 977–980.
6. Lehn, J.-M. Toward Self-Organization and Complex Matter. *Science* **2002**, *295*, 2400–2403.
7. Liu, K.; Kang, Y.; Wang, Z.; Zhang, X. 25th Anniversary Article: Reversible and Adaptive Functional Supramolecular Materials: "Noncovalent Interaction" Matters. *Adv. Mater.* **2013**, *25*, 5530–5548.
8. Rybtchinski, B. Adaptive Supramolecular Nanomaterials Based on Strong Noncovalent Interactions. *ACS Nano* **2011**, *5*, 6791–6818.
9. So, S. M.; Moozeh, K.; Lough, A. J.; Chin, J. Highly Stereoselective Recognition and Deracemization of Amino Acids by Supramolecular Self-Assembly. *Angew. Chem., Int. Ed.* **2014**, *53*, 829–832.
10. Zhang, M.; Yan, X.; Huang, F.; Niu, Z.; Gibson, H. W. Stimuli-Responsive Host-Guest Systems based on the Recognition of Cryptands by Organic Guests. *Acc. Chem. Res.* **2014**, *47*, 1995–2005.
11. Muraoka, T.; Endo, T.; Tabata, K. V.; Noji, H.; Nagatoishi, S.; Tsumoto, K.; Li, R.; Kinbara, K. Reversible Ion Transportation Switch by a Ligand-Gated Synthetic Supramolecular Ion Channel. *J. Am. Chem. Soc.* **2014**, *136*, 15584–15595.
12. Si, W.; Chen, L.; Hu, X. B.; Tang, G. F.; Chen, Z. X.; Hou, J.-L.; Li, Z.-T. Selective Artificial Transmembrane Channels for Protons by Formation of Water Wires. *Angew. Chem., Int. Ed.* **2011**, *50*, 12564–12568.
13. Song, W. J.; Tezcan, F. A. A Designed Supramolecular Protein Assembly with *in vivo* Enzymatic Activity. *Science* **2014**, *346*, 1525–1528.
14. Zhang, C.; Xue, X.; Luo, Q.; Li, Y.; Yang, K.; Zhuang, X.; Jiang, Y.; Zhang, J.; Liu, J.; Zou, G.; et al. Self-Assembled Peptide Nanofibers Designed as Biological Enzymes for Catalyzing Ester Hydrolysis. *ACS Nano* **2014**, *8*, 11715–11723.
15. Choi, I. S.; Bowden, N.; Whitesides, G. M. Macroscopic, Hierarchical, Two-Dimensional Self-Assembly. *Angew. Chem., Int. Ed.* **1999**, *38*, 3078–3081.
16. Zhao, Y.; Sakai, F.; Su, L.; Liu, Y.; Wei, K.; Chen, G.; Jiang, M. Progressive Macromolecular Self-Assembly: From Biomimetic Chemistry to Bio-Inspired Materials. *Adv. Mater.* **2013**, *25*, 5215–5256.
17. Aida, T.; Meijer, E. W.; Stupp, S. I. Functional Supramolecular Polymers. *Science* **2012**, *335*, 813–817.
18. Lehn, J.-M. From Supramolecular Chemistry towards Constitutional Dynamic Chemistry and Adaptive Chemistry. *Chem. Soc. Rev.* **2007**, *36*, 151–160.
19. Houbenov, N.; Nykänen, A.; Iatrou, H.; Hadjichristidis, N.; Ruokolainen, J.; Faul, C. F. J.; Ikkala, O. Fibrillar Constructs from Multilevel Hierarchical Self-Assembly of Discotic and Calamitic Supramolecular Motifs. *Adv. Funct. Mater.* **2008**, *18*, 2041–2047.
20. Jin, H.; Zhou, Y.; Huang, W.; Yan, D. Polymerization-like Multilevel Hierarchical Self-Assembly of Polymer Vesicles into Macroscopic Superstructures with Controlled Complexity. *Langmuir* **2010**, *26*, 14512–14519.
21. Elemans, J. A. A. W.; Rowan, A. E.; Nolte, R. J. M. Mastering molecular matter. Supramolecular Architectures by Hierarchical Self-Assembly. *J. Mater. Chem.* **2003**, *13*, 2661–2670.
22. Ikkala, O.; ten Brinke, G. Hierarchical Self-Assembly in Polymeric Complexes: Towards Functional Materials. *Chem. Commun.* **2004**, 2131–2137.
23. Potschka, M.; Koch, M. H. J.; Adams, M. L.; Schuster, T. M. Time-Resolved Solution X-Ray Scattering of Tobacco Mosaic Virus Coat Protein: Kinetics and Structure of Intermediates. *Biochemistry* **1988**, *27*, 8481–8491.
24. Ottani, V.; Martini, D.; Franchi, M.; Ruggeri, A.; Raspanti, M. Hierarchical Structures in Fibrillar Collagens. *Micron* **2002**, *33*, 587–596.
25. O'Sullivan, A. Cellulose: The Structure Slowly Unravels. *Cellulose* **1997**, *4*, 173–207.
26. Hanisch, A.; Gröschel, A. H.; Förtsch, M.; Drechsler, M.; Jinnai, H.; Ruhland, T. M.; Schacher, F. H.; Müller, A. H. E. Counterion-Mediated Hierarchical Self-Assembly of an ABC Miktoarm Star Terpolymer. *ACS Nano* **2013**, *7*, 4030–4041.
27. Rizis, G.; van de Ven, T. G. M.; Eisenberg, A. Raft" Formation by Two-Dimensional Self-Assembly of Block Copolymer Rod Micelles in Aqueous Solution. *Angew. Chem., Int. Ed.* **2014**, *53*, 9000–9003.
28. Lee, S. J.; Hupp, J. T.; Nguyen, S. T. Growth of Narrowly Dispersed Porphyrin Nanowires and Their Hierarchical Assembly into Macroscopic Columns. *J. Am. Chem. Soc.* **2008**, *130*, 9632–9633.
29. Li, H.; Sun, H.; Qi, W.; Xu, M.; Wu, L. Onionlike Hybrid Assemblies Based on Surfactant-Encapsulated Polyoxometalates. *Angew. Chem., Int. Ed.* **2007**, *46*, 1300–1303.
30. Wu, H.; Thalladi, V. R.; Whitesides, S.; Whitesides, G. M. Using Hierarchical Self-Assembly to Form Three-Dimensional Lattices of Spheres. *J. Am. Chem. Soc.* **2002**, *124*, 14495–14502.

31. Decher, G. Fuzzy Nanoassemblies: Toward Layered Polymeric Multicomposites. *Science* **1997**, *277*, 1232–1237.
32. Borges, J.; Mano, J. F. Molecular Interactions Driving the Layer-by-Layer Assembly of Multilayers. *Chem. Rev.* **2014**, *114*, 8883–8942.
33. Zhang, X.; Chen, H.; Zhang, H. Y. Layer-by-Layer Assembly: From Conventional to Unconventional Methods. *Chem. Commun.* **2007**, 1395–1405.
34. Schlenoff, J. B. Retrospective on the Future of Polyelectrolyte Multilayers. *Langmuir* **2009**, *25*, 14007–14010.
35. Du, Y.; Luna, L. E.; Tan, T. W.; Rubner, M. F.; Cohen, R. E. Hollow Silica Nanoparticles in UV Visible Antireflection Coatings for Poly(Methyl Methacrylate) Substrates. *ACS Nano* **2010**, *4*, 4308–4316.
36. Jisr, R. M.; Rmaile, H. H.; Schlenoff, J. B. Hydrophobic and Ultrahydrophobic Multilayer Thin Films from Perfluorinated Polyelectrolytes. *Angew. Chem., Int. Ed.* **2005**, *44*, 782–785.
37. Li, Y.; Li, L.; Sun, J. Bioinspired Self-Healing Superhydrophobic Coatings. *Angew. Chem., Int. Ed.* **2010**, *49*, 6129–6133.
38. Ma, Y.; Zhang, Y.; Wu, B.; Sun, W.; Li, Z.; Sun, J. Polyelectrolyte Multilayer Films for Building Energetic Walking Devices. *Angew. Chem., Int. Ed.* **2011**, *50*, 6254–6257.
39. South, A. B.; Lyon, L. A. Autonomic Self-Healing of Hydrogel Thin Films. *Angew. Chem., Int. Ed.* **2010**, *49*, 767–771.
40. Kim, B.-S.; Park, S. W.; Hammond, P. T. Hydrogen-Bonding Layer-by-Layer-Assembled Biodegradable Polymeric Micelles as Drug Delivery Vehicles from Surfaces. *ACS Nano* **2008**, *2*, 386–392.
41. Hu, X.; Ji, J. Covalent Layer-by-Layer Assembly of Hyperbranched Polyether and Polyethyleneimine: Multilayer Films Providing Possibilities for Surface Functionalization and Local Drug Delivery. *Biomacromolecules* **2011**, *12*, 4264–4271.
42. Park, M.-K.; Deng, S.; Advincula, R. C. pH-Sensitive Bipolar Ion-Permselective Ultrathin Films. *J. Am. Chem. Soc.* **2004**, *126*, 13723–13731.
43. Bruening, M. L.; Sullivan, D. M. Enhancing the Ion-Transport Selectivity of Multilayer Polyelectrolyte Membranes. *Chem. - Eur. J.* **2002**, *8*, 3833–3837.
44. Ji, Q.; Yoon, S. B.; Hill, J. P.; Vinu, A.; Yu, J.-S.; Ariga, K. Layer-by-Layer Films of Dual-Pore Carbon Capsules with Designable Selectivity of Gas Adsorption. *J. Am. Chem. Soc.* **2009**, *131*, 4220–4221.
45. Pavlukhina, S. V.; Kaplan, J. B.; Xu, L.; Chang, W.; Yu, X.; Madhyastha, S.; Yakandawala, N.; Mentbayeva, A.; Khan, B.; Sukhishvili, S. A. Noneluting Enzymatic Antibiofilm Coatings. *ACS Appl. Mater. Interfaces* **2012**, *4*, 4708–4716.
46. Podsiadlo, P.; Kaushik, A. K.; Arruda, E. M.; Waas, A. M.; Shim, B. S.; Xu, J.; Nandivada, H.; Pumplin, B. G.; Lahann, J.; Ramamoorthy, A.; et al. Ultrastrong and Stiff Layered Polymer Nanocomposites. *Science* **2007**, *318*, 80–83.
47. Li, Y.-C.; Schulz, J.; Mannen, S.; Delhom, C.; Condon, B.; Chang, S.; Zammarano, M.; Grunlan, J. C. Flame Retardant Behavior of Polyelectrolyte-Clay Thin Film Assemblies on Cotton Fabric. *ACS Nano* **2010**, *4*, 3325–3337.
48. Shchukin, D. G.; Möhwald, H. Smart Nanocontainers as Depot Media for Feedback Active Coatings. *Chem. Commun.* **2011**, *47*, 8730–8739.
49. Kharlampieva, E.; Kozlovskaya, V.; Sukhishvili, S. A. Layer-by-Layer Hydrogen-Bonded Polymer Films: From Fundamentals to Applications. *Adv. Mater.* **2009**, *21*, 3053–3065.
50. Ogawa, Y.; Arikawa, Y.; Kida, T.; Akashi, M. Fabrication of Novel Layer-by-Layer Assembly Films Composed of Poly(lactic acid) and Polylysine through Cation-Dipole Interactions. *Langmuir* **2008**, *24*, 8606–8609.
51. Guo, Y.; Geng, W.; Sun, J. Layer-by-Layer Deposition of Polyelectrolyte-Polyelectrolyte Complexes for Multilayer Film Fabrication. *Langmuir* **2009**, *25*, 1004–1010.
52. Cho, J.; Quinn, J. F.; Caruso, F. Fabrication of Polyelectrolyte Multilayer Films Comprising Nanoblended Layers. *J. Am. Chem. Soc.* **2004**, *126*, 2270–2271.
53. Li, Y.; Wang, X.; Sun, J. Layer-by-Layer Assembly for Rapid Fabrication of Thick Polymeric Films. *Chem. Soc. Rev.* **2012**, *41*, 5998–6009.
54. Picart, C.; Mutterer, J.; Richert, L.; Luo, Y.; Prestwich, G. D.; Schaaf, P.; Voegel, J.-C.; Lavalle, P. Molecular Basis for the Explanation of the Exponential Growth of Polyelectrolyte Multilayers. *Proc. Natl. Acad. Sci. U. S. A.* **2002**, *99*, 12531–12535.
55. Cho, J.; Char, K.; Hong, J.-D.; Lee, K.-B. Fabrication of Highly Ordered Multilayer Films Using a Spin Self-Assembly Method. *Adv. Mater.* **2001**, *13*, 1076–1078.
56. Schlenoff, J. B.; Dubas, S. T.; Farhat, T. Sprayed Polyelectrolyte Multilayers. *Langmuir* **2000**, *16*, 9968–9969.
57. Lee, J.-H.; Hwang, H. J.; Bhak, G.; Jang, Y.; Paik, S. R.; Char, K. *In situ* Fibril Formation of κ-Casein by External Stimuli within Multilayer Thin Films. *ACS Macro Lett.* **2013**, *2*, 688–693.
58. Li, Y.; Chen, S.; Wu, M.; Sun, J. All Spraying Processes for the Fabrication of Robust, Self-Healing, Superhydrophobic Coatings. *Adv. Mater.* **2014**, *26*, 3344–3348.
59. Liu, X.; Zhou, L.; Liu, F.; Ji, M.; Tang, W.; Pang, M.; Sun, J. Exponential Growth of Layer-by-Layer Assembled Coatings with Well-Dispersed Ultrafine Nanofillers: A Facile Route to Scratch-Resistant and Transparent Hybrid Coatings. *J. Mater. Chem.* **2010**, *20*, 7721–7727.
60. Zhang, L.; Sun, J. Layer-by-Layer Deposition of Polyelectrolyte Complexes for the Fabrication of Foam Coatings with High Loading Capacity. *Chem. Commun.* **2009**, 3901–3903.
61. Wang, Z.; Möhwald, H.; Gao, C. Nanotubes Protruding from Poly(allylamine hydrochloride)-Graft-Pyrene Microcapsules. *ACS Nano* **2011**, *5*, 3930–3936.
62. Sadasivan, S.; Köhler, K.; Sukhorukov, G. B. Fabrication of Organized Porphyrin-Nanotube-Attached Heat-Sensitive Polyelectrolyte Capsules. *Adv. Funct. Mater.* **2006**, *16*, 2083–2088.
63. Shiratori, S. S.; Rubner, M. F. pH-Dependent Thickness Behavior of Sequentially Adsorbed Layers of Weak Polyelectrolytes. *Macromolecules* **2000**, *33*, 4213–4219.
64. Chia, K.-K.; Rubner, M. F.; Cohen, R. E. pH-Responsive Reversibly Swellable Nanotube Arrays. *Langmuir* **2009**, *25*, 14044–14052.